



## Experimental and Prediction Using Artificial Neural Network of Bed Porosity and Solid Holdup in Viscous 3-Phase Inverse Fluidization

**Amer A. Abdulrahman**

*Department of Chemical Engineering/ University of Technology*

Email: [ameraa1972@yahoo.com](mailto:ameraa1972@yahoo.com)

(Received 2 February 2016; accepted 27 March 2016)

### Abstract

In the present investigation, bed porosity and solid holdup in viscous three-phase inverse fluidized bed (TPIFB) are determined for aqueous solutions of carboxy methyl cellulose (CMC) system using polyethylene and polypropylene as a particles with low-density and diameter (5 mm) in a (9.2 cm) inner diameter with height (200 cm) of vertical perspex column. The effectiveness of gas velocity  $U_g$ , liquid velocity  $U_L$ , liquid viscosity  $\mu_L$ , and particle density  $\rho_s$  on bed porosity  $B_p$  and solid holdups  $\varepsilon_g$  were determined. The bed porosity increases with "increasing gas velocity", "liquid velocity", and "liquid viscosity". Solid holdup decreases with increasing gas, liquid velocities and liquid viscosity. Solid holdup with "low density particles" shows a higher numerical quantity "than that in the beds" with "high density". Levenberg-Marquardt back propagation of "artificial neural network (ANNs)" was utilized to predict the bed porosity and solid holdup. The expected values are in an excellent relationship with the experimental values, where the advanced model is high-fidelity and own a large capacity to predict bed porosity and solid holdup.

**Keywords:** *bed porosity, solid holdup, three phase, inverse fluidization, ANNs.*

### 1. Introduction

A three phase (gas – liquid – solid) inverse fluidized bed (TPIFB) is an operation where continuous liquid phase is introduced from the upper of the column in the opposite direction to the continuing flow of gas which is introduced from the bottom and the particles with low density expand down. Applications of (TPIFB) have been increased because, low pressure drop, higher mass and heat transfer rates, low-level operating costs and higher efficiency contact between various phases [1-2]. Three phase fluidized beds are used in petrochemical processing, chemical processing, biochemical processing, hydrogenation and hydro de-sulfurization of residual oil, facilitating catalytic and non-catalytic reactions [3-4].

To understand the phenomena of three phase fluidized bed, important parameters must be described such as: bed pressure drop, minimum

fluidization velocity, bed porosity, gas holdup, liquid holdup and solid holdup. The hydrodynamic characteristics of (TPIFB) have been studied by many researchers. Fluid flow rate (as gas phase and liquid phase), particle density (as solid phase) and bed height are important variables affecting the quality of fluidization [5]. The hydrodynamics of 3-phase fluidized bed was studied with different sizes of particle and liquid as a continuous phase [6]. It was found that the gas holdup and bed porosity increase with increasing gas flow rate. Gas holdup, minimum fluidization velocity, physical properties of liquid are measured for three phase fluidized bed system by using a perforated teflon plate as a gas distributor, different types of a non-Newtonian (pseudo plastic) liquids as a liquid phase, different types of gases as gas phase and activated carbon with different diameters as solid phase [7].

Air was used as the gas phase, water as liquid phase, and low density particle (wood) as solid were employed to study the hydrodynamic characteristics of 3-phase fluidized bed phase [8]. Two types of low density particles were used to investigate the hydrodynamic characteristics of (TPIFB) [9]. In Newtonian (aqueous solutions of glycerol) and non-Newtonian (aqueous solutions of carboxyl methyl cellulose) 3-phase inverse fluidized bed, bed porosity and solid holdup were studied by using polyethylene and polypropylene particles of different diameters [10].

A feed forward neural network, Multilayer Perceptron was used for chemical engineering utilization which consists of multilayer hierarchical structure, input, output layers, and at least one layer called (hidden) of processing units between them. Artificial neural networks (ANNs) prepare correlation between input and output variables. The schematic of the MLP network with two hidden layers is as shown in figure (1).

There are a broad range of variables such as the expansion of the bed, gas, liquid and solid holdups for gas-liquid- solid fluidized bed has been used to generalize various relationships between the data of non-linear parameters [11].

Polyethylene hollow spheres, water and air are used experimentally in (TPIFB) to find solute concentration and mass transfer coefficient. By using (ANNs), the data produced was used for providing models [12]. Four different non-Newtonian liquids and four different polymeric solids in single and binary system inverse fluidized beds are used to study and develop empirical correlation for the bed expansion. A multilayer perceptron trained with back propagation and Levenberg -Marquardt algorithms has been used for the Artificial Neural Network (ANN) analysis because "trainlm is a network training function that updates weight and bias values according to Levenberg-Marquardt optimization. Trainlm is often the fastest backpropagation algorithm in the toolbox, and is highly recommended as a first-choice supervised algorithm, although it does require more memory than other" [13].

The aim of the present work, experimental data was use to develop a mathematic model to estimate solid holdup and bed porosity as  $U_g$ ,  $U_L$ ,  $\mu_L$ , and  $\rho_s$ .

## 2. Experimental Work

The Planned laboratory design of experimental apparatus is exhibited in Figure (2).

Practical experiments were carrying on in a vertical column made of Perspex (0.092 m) internal diameter and (2m) height. The air was introduced from the lower of the column via the gas distributor. The liquid phase was fed from the top of the column through a (3cm) tube from the liquid tank. The distributor of the liquid holds (48) evenly spaced holes, with diameter (2.5 mm) for each, while the gas distributor holds (26) evenly spaced holes, with diameter of (2mm) for each. Individual phase holdup was determined by static pressure drop method based on the cognition of the particles height, pressure drop and the physical properties of the three phases. Six taps of pressure are equally spaced (21.5cm) interval on the exterior wall of the part section; First tap was placed (5cm) from the water distributor on the top of the column. Manometers are used to measure the pressure drop inside the column. The pressure drop was measured with water velocity ranging from fixed condition to fluidization. Air was supplied by air compressor capable of delivering about (5) bar. The air velocity was measured with Rota meter ranging from (0.05-0.75) m/s.

Water was supplied by liquid reservoir with ( $0.1m^3$ ) in volume which was connected to water pump with ( $5.4 m^3/hr.$  and (46m) H.max. The water velocity was measured with flow meter ranging from (0.01- 0.06) m/s. Two different solid spheres were used as solid phase made of polyethylene and polypropylene beads with average diameter of (5 mm). Table (1) shows the physical characteristics of the solid particles as solid phase. As a liquid phase pure water and three different carboxy methyl cellulose solutions (CMC) were applied. Table (2) shows the operating conditions and physical characteristics of the liquid. A brookfield synchroelectric rotational viscometer was used to determine the viscosity ( $\mu_L$ ) of "liquid phase". Air was used as a "gas phase and" its properties are shown in Table (3).

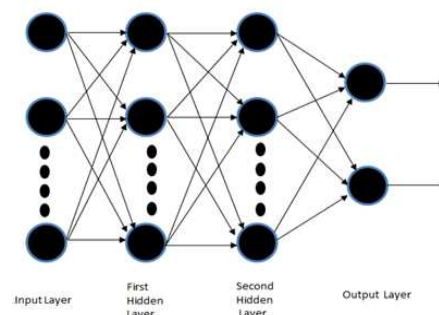
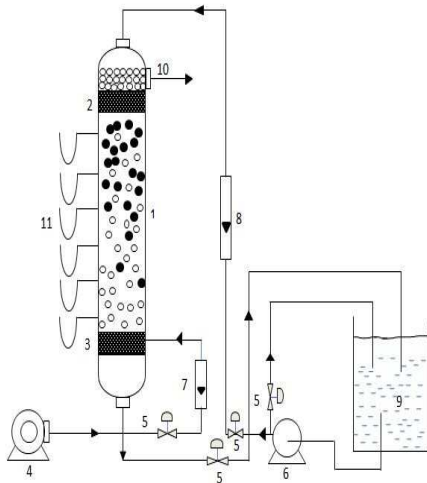


**Fig. 1. Artificial Neural Network (ANNs) (Multilayer Perceptron).**



1- Liquid column, 2- Liquid distributor, 3- gas distributor 4- Air compressor, 5- Needle valve, 6- Liquid pump, 7- Gas flow meter, 8- Liquid flow meter, 9- Reservoir tank, 10- Vent line, 11- U tube manometer.

Fig. 2. Experimental apparatus.

Table 1, Physical Properties of Particles as Solid Phase.

Solid Phase	Shape	Average diameter (mm)	Density (kg/m <sup>3</sup> )
Polypropylene	spheres	5	875
Polyethylene	spheres	5	969

Table 2, Properties of Liquid phase.

Liquid Phase	Density (kg/m <sup>3</sup> )	Viscosity *10 <sup>3</sup> (Pa.s)
Water	1000	0.97
Water-CMC (0.1 wt. %)	1001	9.5
Water-CMC (0.3 wt. %)	1004	35
Water-CMC (0.5 wt. %)	1006	49.5

Table 3, Properties of Gas Phase.

Gas Phase	Density (Kg/m <sup>3</sup> )	Viscosity *10 <sup>5</sup> (Kg/m.sec)
Air	1.19	1.6

Table 4, The limit of the input parameters in ANN.

Inputs		Range
Gas velocity	(m/s)	0.05 – 0.75
liquid velocity	(m/s)	0.01 – 0.06
Liquid viscosity *10 <sup>3</sup>	(Pa.s)	0.97 - 49.5
Particles density	(kg/m <sup>3</sup> )	875 - 969

ANN is utilized to predict bed porosity and solid holdup under using Matlab 7.10 software. The data of experiments can be divided into two sections, training and testing, and eventually trains the ANNs is built according to the specific data was trained to compute the achievement of the training results by using mean square error (MSE) and the linear regressions (R<sup>2</sup>) [14, 15].

$$"MSE = 1/n \sum_{t=1}^n (T_j - Y_j)^2 "$$
 ... (1)

$$"R^2 = 1 - \left[ \frac{\sum_j (T_j - Y_j)^2}{\sum_j (Y_j)^2} \right] "$$
 ... (2)

(T) act as a target value, where (Y) act as an output value, and (n) act as a pattern.

For present work, Levenberg-Marquardt backpropagation training algorithm is in use to train the network, for training artificial neural networks 270 of 384 data are in use and for testing aim 114 data are in use with log-sigmoid hidden neurons and linear output neurons. 3- Layers feed forward network are in use as the network, one for input layer, tow for hidden layer, and one for output layer. The input layer has 4 neurons (gas velocity, liquid velocity, density of the particles, and liquid viscosity), as in the case of hidden layers distributed 8 neutrons in the first one, four neutrons in the second layer and output layer has two neurons (bed porosity and solid holdup). The network was then trained to predict the bed porosity and solid holdup as outputs. Table (4) presents the limit of the input parameters in ANN.

Neurons are placed at the input layer in the feed forward networks towards output layer so that layers and transference from first layer to another one. The obtained data are change position from the beginning from input layer to the tow hidden layers and in the end sent to the output layer to be there to deal with the data for the final results and then sent out. Figure (3) exhibit a feed forward ANN for two hidden layers as utilized in present study.

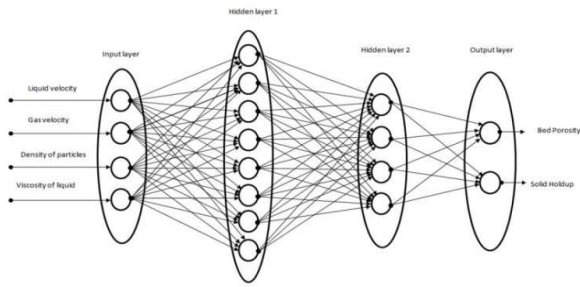


Fig. 3. Multilayer neural network.

### 3. Results & Discussion

#### 3.1 Effect of Superficial Gas Velocity ( $U_g$ )

In the present study, the variations of bed porosity ( $B_p$ ) with superficial gas velocity ( $U_g$ ) are shown in figures (4-5) using polyethylene particle with liquid phase viscosity  $9.5 \times 10^{-3}$  and  $49.5 \times 10^{-3}$  Pa.s respectively. The bed expansion and the total volume of fluidized bed increased with an increase in airflow rate, therefore the bed porosity also increased in inverse three phase fluidized bed. The accepted explanation is as follows the bubbles are broken by the large inertia of particles. Typical examples of bed porosity can be seen in figures (6-7) for

polypropylene particles with liquid phase viscosity  $9.5 \times 10^{-3}$  and  $35 \times 10^{-3}$  Pa.s respectively and figures (8-9) for polyethylene and polypropylene particles with pure water as liquid phase respectively. The values of the bed porosity of light particles are smaller than those for heavy particles [3, 16, and 17].

The effects of  $U_g$  on the  $\epsilon_s$  are shown in figures (10-11) for polyethylene particles with viscosity of  $9.5 \times 10^{-3}$  and  $49.5 \times 10^{-3}$  Pa.s of liquid phase respectively. The bed in the column expands when the  $U_g$  increases, therefore increasing in the liquid and gas holdups which results decreasing in the  $\epsilon_s$ . As can be seen in these figures, the polypropylene owns solid holdup greater than that of the polyethylene. This is because the polypropylene has density lower than that of the polyethylene. This phenomenon is due to the beds of light particles which cannot expand easily in THIFB because of the influence of the buoyant force affecting the particles. Typical examples of solid holdup can be seen in figures (12-13) for polypropylene particle with liquid phase viscosity  $9.5 \times 10^{-3}$  and  $49.5 \times 10^{-3}$  Pa.s respectively and figures (14-15) for polyethylene and polypropylene particles with pure water as liquid phase respectively [2,5,16,17].

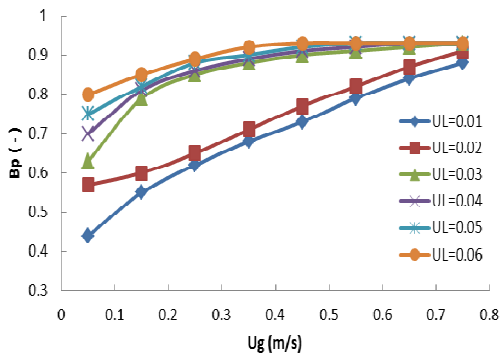


**Fig. 4. Influence of Ug on Bp**  
 Particle: Polyethylene;  $\rho_s = 969$  [kg/m<sup>3</sup>];  
 $\mu_L = 0.95 \times 10^{-2}$  [Pa.s].

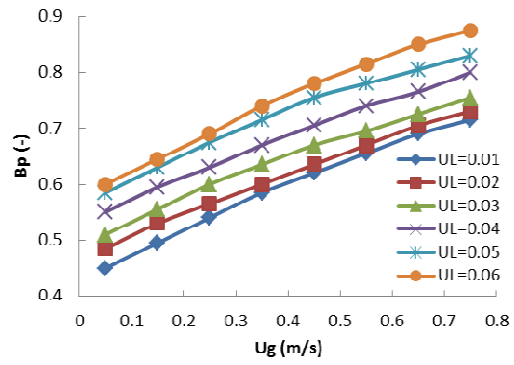


**Fig. 7. Influence of Ug on Bp**  
 Particle: Polypropylene;  $\rho_s = 875$  [kg/m<sup>3</sup>];  
 $\mu_L = 3.5 \times 10^{-2}$  [Pa.s].

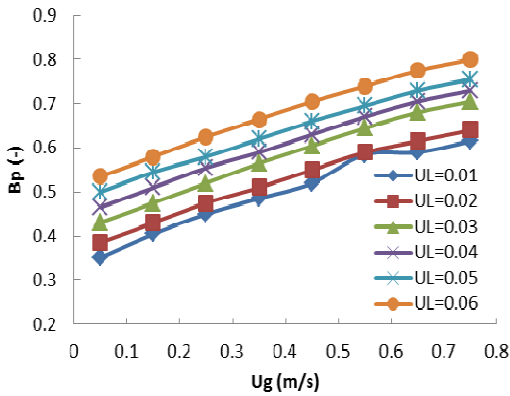


**Fig. 5. Influence of Ug on Bp**  
 Particle: Polyethylene;  $\rho_s = 969$  [kg/m<sup>3</sup>];  
 $\mu_L = 4.95 \times 10^{-2}$  [Pa.s].

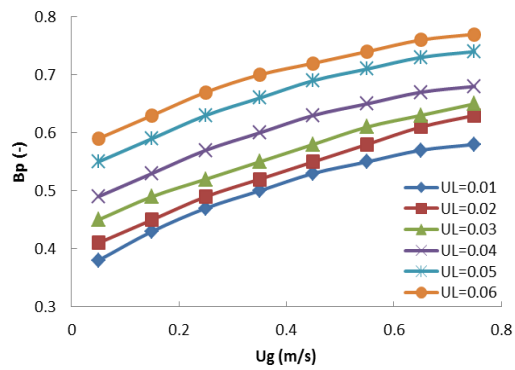


**Fig. 8. Influence of Ug on Bp**  
 Particle: Polyethylene;  $\rho_s = 969$  [kg/m<sup>3</sup>];  
 Pure water;  $\mu_L = 0.097 \times 10^{-2}$  [Pa.s].

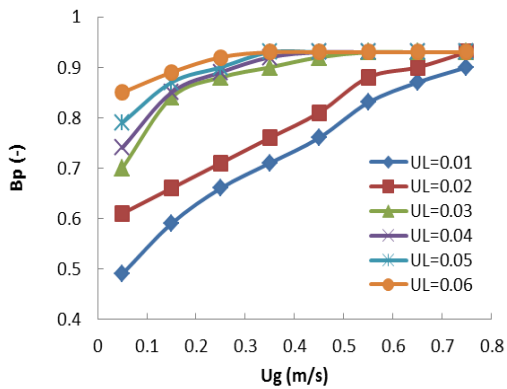


**Fig. 6. Influence of Ug on Bp**  
 Particle: Polypropylene;  $\rho_s = 875$  [kg/m<sup>3</sup>];  
 $\mu_L = 0.95 \times 10^{-2}$  [Pa.s].

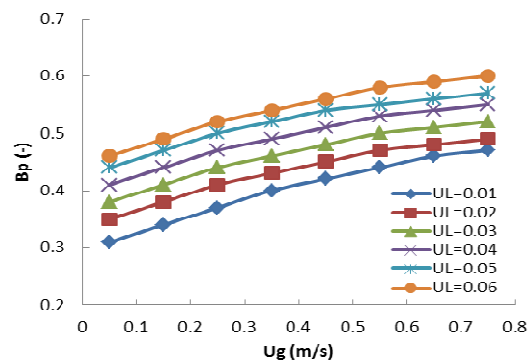


**Fig. 9. Influence of Ug on Bp**  
 Particle: Polypropylene;  $\rho_s = 875$  [kg/m<sup>3</sup>];  
 Pure water;  $\mu_L = 0.097 \times 10^{-2}$  [Pa.s].

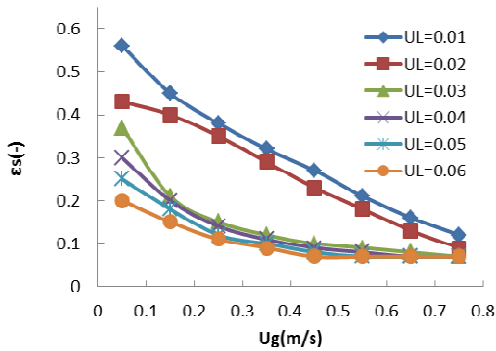


**Fig. 10. Influence of Ug on εg**  
 Particle: Polyethylene;  $\rho_s = 969 \text{ [kg/m}^3\text{]}$ ;  
 $\mu_L = 0.95 \times 10^{-2} \text{ [Pa.s]}$ .

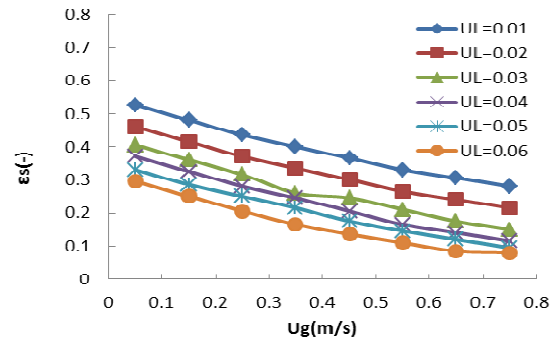


**Fig. 13. Influence of Ug on εg**  
 Particle: Polypropylene;  $\rho_s = 875 \text{ [kg/m}^3\text{]}$ ;  
 $\mu_L = 4.95 \times 10^{-2} \text{ [Pa.s]}$ .

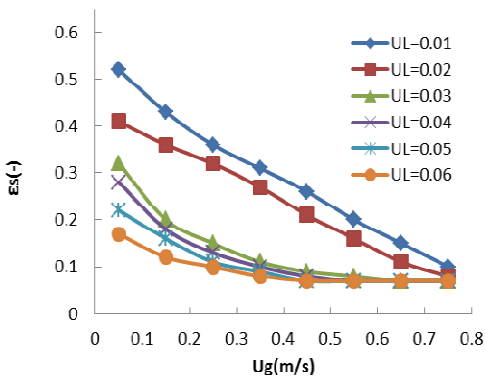


**Fig. 11. Influence of Ug on εg**  
 Particle: Polyethylene;  $\rho_s = 969 \text{ [kg/m}^3\text{]}$ ;  
 $\mu_L = 4.95 \times 10^{-2} \text{ [Pa.s]}$ .

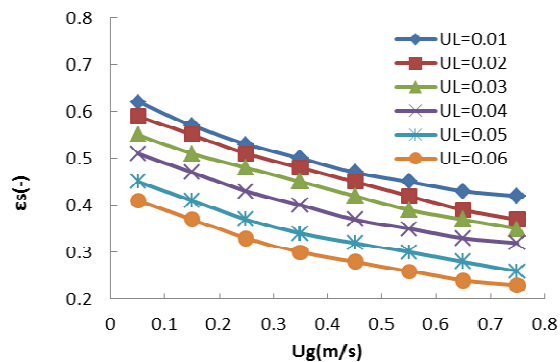


**Fig. 14. Influence of Ug on εg**  
 Particle: Polyethylene;  $\rho_s = 969 \text{ [kg/m}^3\text{]}$ ;  
 Pure water;  $\mu_L = 0.097 \times 10^{-2} \text{ [Pa.s]}$ .

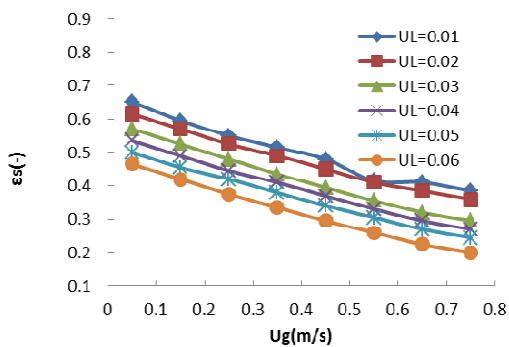


**Fig. 12. Influence of Ug on εg**  
 Particle: Polypropylene;  $\rho_s = 875 \text{ [kg/m}^3\text{]}$ ;  
 $\mu_L = 0.95 \times 10^{-2} \text{ [Pa.s]}$ .

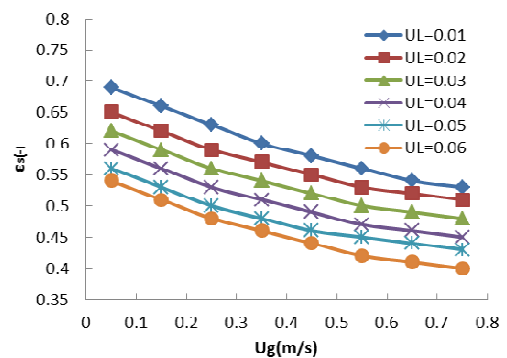


**Fig. 15. Influence of Ug on εg**  
 Particle: Polypropylene;  $\rho_s = 875 \text{ [kg/m}^3\text{]}$ ;  
 Pure water;  $\mu_L = 0.097 \times 10^{-2} \text{ [Pa.s]}$ .

### 3.2 Effect of Superficial Liquid Velocity ( $U_L$ )

The effect of superficial liquid velocity ( $U_L$ ) on the bed porosity ( $B_p$ ) is represented in figures

(16 – 17) for polyethylene particles with liquid phase viscosity  $35 \times 10^{-3}$  and  $49.5 \times 10^{-3} \text{ Pa.s}$  respectively. As can be seen from these figures, the bed porosity increases with increasing superficial liquid velocity. This can be due to the

fact that the gas holdup and liquid holdup increase gradually with increasing  $U_L$  in a given gas velocity. This event could be due to the fact that the liquid phase flows moving down against the buoyance force act on the particles. A similar trend is observed in the figures (18 - 19) for the beds of polypropylene particles with viscosity of  $35 \times 10^{-3}$  and  $49.5 \times 10^{-3}$  Pa.s respectively and figures (20-21) for polyethylene and polypropylene particles with pure water as liquid phase respectively.

In the present study, figures (22 – 23) give the variation of solid holdup with superficial liquid

velocity for polyethylene particles with liquid phase viscosity  $35 \times 10^{-3}$  and  $49.5 \times 10^{-3}$  Pa.s respectively. In these figures, the  $(\epsilon_g)$  decreases with increasing  $U_L$ , as a results of increased liquid and gas holdups [2, 5]. The same trend can be seen in the bed of polypropylene particle with liquid phase viscosity  $35 \times 10^{-3}$  and  $49.5 \times 10^{-3}$  Pa.s respectively in figures (24-25) and in figures (26-27) for polyethylene and polypropylene particles with pure water as liquid phase respectively.

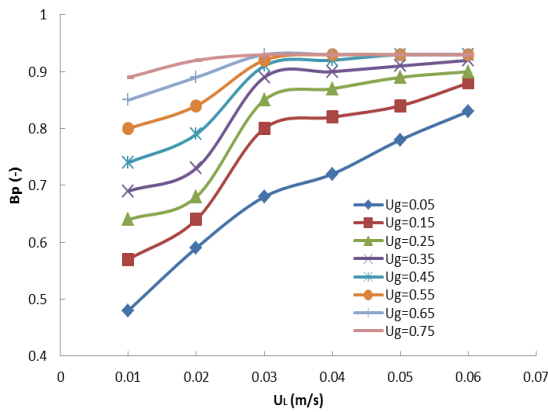


**Fig. 16. Influence of  $U_L$  on Bp**  
**Particle: Polyethylene;  $\rho_s = 969$  [kg/m<sup>3</sup>];**  
 **$\mu_L = 3.5 \times 10^{-2}$  [Pa.s].**

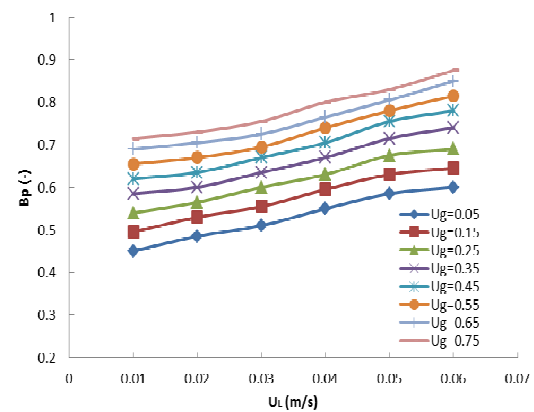


**Fig. 18. Influence of  $U_L$  on Bp**  
**Particle: Polypropylene;  $\rho_s = 875$  [kg/m<sup>3</sup>];**  
 **$\mu_L = 3.5 \times 10^{-2}$  [Pa.s].**

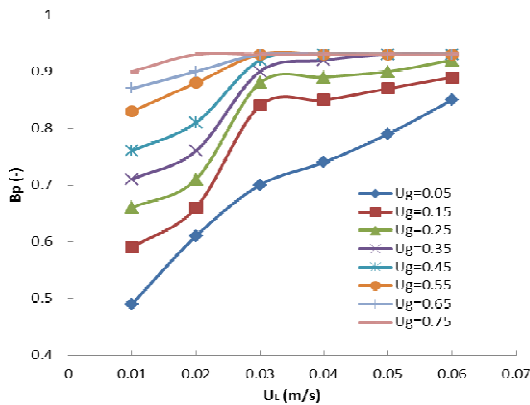


**Fig. 17. Influence of  $U_L$  on Bp**  
**Particle: Polyethylene;  $\rho_s = 969$  [kg/m<sup>3</sup>];**  
 **$\mu_L = 4.95 \times 10^{-2}$  [Pa.s].**

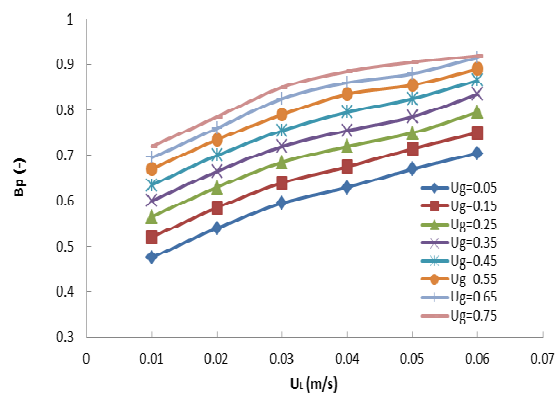


**Fig. 19. Influence of  $U_L$  on Bp**  
**Particle: Polypropylene;  $\rho_s = 875$  [kg/m<sup>3</sup>];**  
 **$\mu_L = 4.95 \times 10^{-2}$  [Pa.s].**

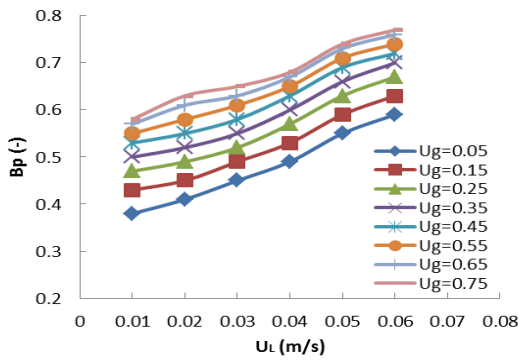


**Fig. 20. Influence of  $U_L$  on  $B_p$**   
 Particle: Polyethylene;  $\rho_s = 969$  [kg/m<sup>3</sup>];  
 Pure water;  $\mu_L = 0.097 \times 10^{-2}$  [Pa.s].

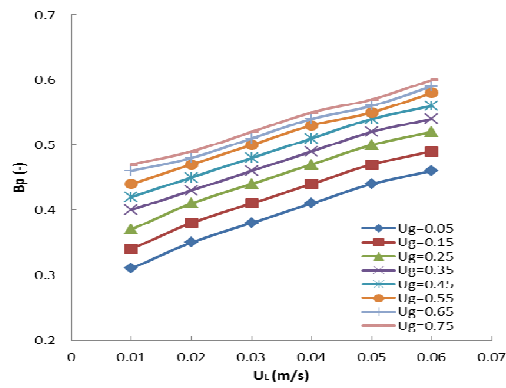


**Fig. 21. Influence of  $U_L$  on  $B_p$**   
 Particle: Polypropylene;  $\rho_s = 875$  [kg/m<sup>3</sup>];  
 Pure water;  $\mu_L = 0.097 \times 10^{-2}$  [Pa.s].

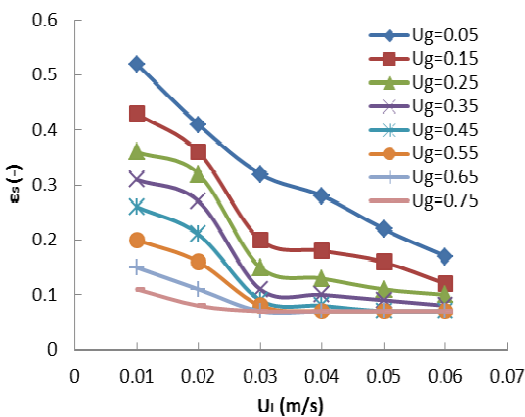


**Fig. 22. Influence of  $U_L$  on  $\epsilon_g$**   
 Particle: Polyethylene;  $\rho_s = 969$  [kg/m<sup>3</sup>];  
 $\mu_L = 3.5 \times 10^{-2}$  [Pa.s].

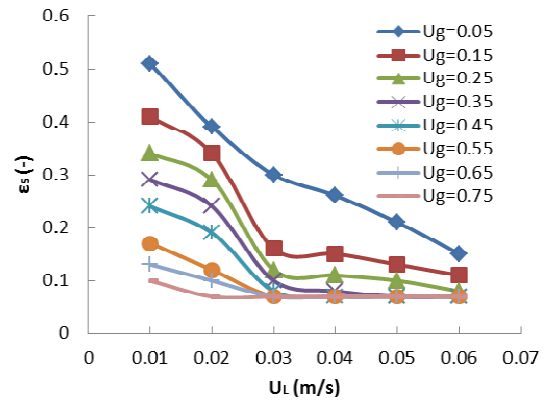


**Fig. 23. Influence of  $U_L$  on  $\epsilon_g$**   
 Particle: Polyethylene;  $\rho_s = 969$  [kg/m<sup>3</sup>];  
 $\mu_L = 4.95 \times 10^{-2}$  [Pa.s].

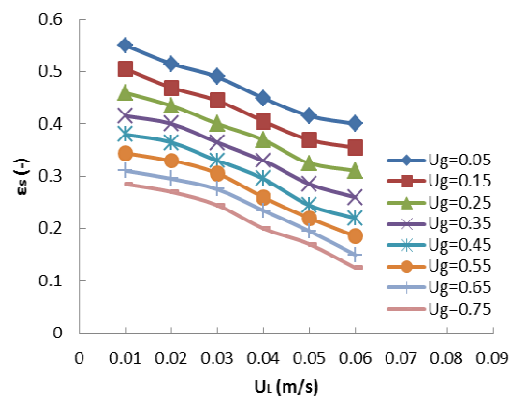


**Fig. 24. Influence of  $U_L$  on  $\epsilon_g$**   
 Particle: Polypropylene;  $\rho_s = 875$  [kg/m<sup>3</sup>];  
 $\mu_L = 3.5 \times 10^{-2}$  [Pa.s].

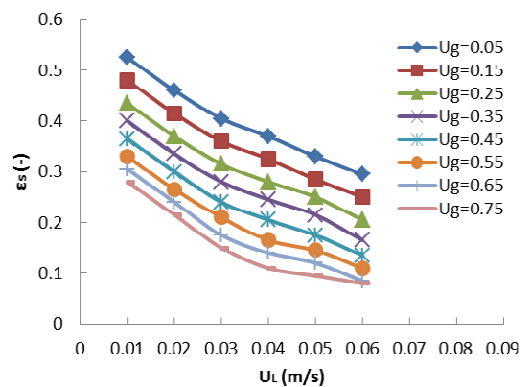


**Fig. 25. Influence of  $U_L$  on  $\epsilon_g$**   
 Particle: Polypropylene;  $\rho_s = 875$  [kg/m<sup>3</sup>];  
 $\mu_L = 4.95 \times 10^{-2}$  [Pa.s].

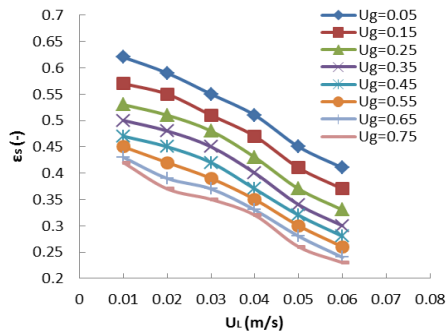


Fig. 26. Influence of  $U_L$  on  $\epsilon_g$  Particle: Polyethylene;  $\rho_s = 969$  [kg/m<sup>3</sup>]; Pure water;  $\mu_L = 0.097 \times 10^{-2}$  [Pa.s].

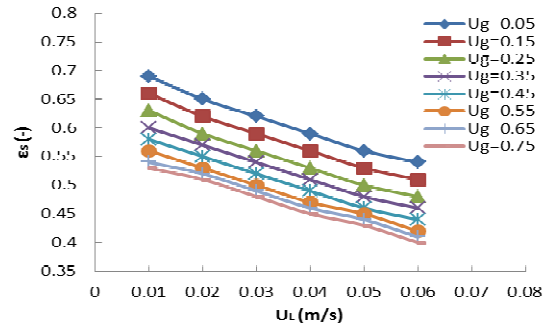


Fig. 27. Influence of  $U_L$  on  $\epsilon_g$  Particle: Polypropylene;  $\rho_s = 875$  [kg/m<sup>3</sup>]; Pure water;  $\mu_L = 0.097 \times 10^{-2}$  [Pa.s].

### 3.3. Effect of Liquid Viscosity ( $\mu_L$ )

Typical plots of bed porosity against liquid viscosity are shown in figures (28 – 29) for polyethylene and polypropylene particles at 0.35 m/s for the gas velocity. As a result of the increase in drag force on the particles when increasing the viscosity of the liquid, gas velocity and liquid

velocity led to the increasing in the porosity of the bed for the inverse fluidized bed.

Effects of liquid viscosity on the solid holdup in the bed are shown in figures (30-31) for polyethylene and polypropylene particles. The particles could be spread out easily by increasing the  $\mu_L$ ; thus the  $\epsilon_s$  decreases with increasing  $\mu_L$  [1, 18].

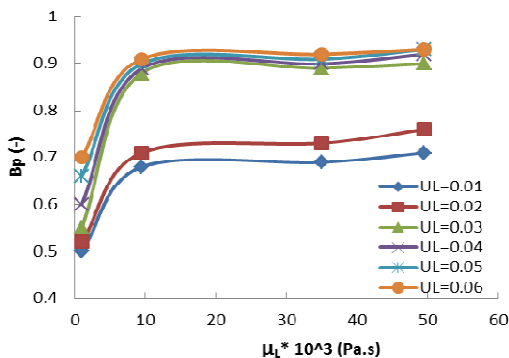


Fig. 28 Influence of  $\mu_L$  on  $B_p$  Particle: Polyethylene;  $\rho_s = 969$  [kg/m<sup>3</sup>];  $U_g = 0.35$  m/s.

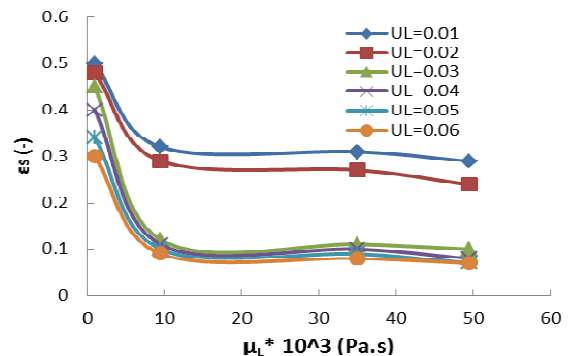


Fig. 30. Influence of  $\mu_L$  on  $\epsilon_g$  Particle: Polyethylene;  $\rho_s = 969$  [kg/m<sup>3</sup>];  $U_g = 0.35$  m/s.

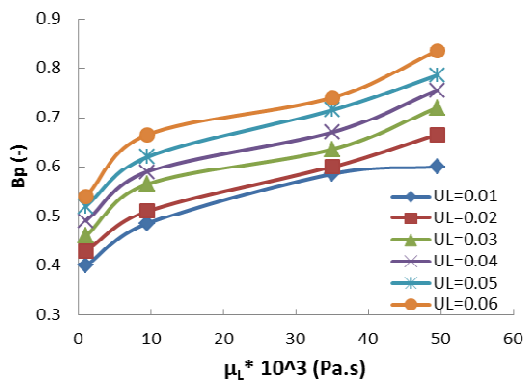


Fig. 29. Influence of  $\mu_L$  on  $B_p$  Particle: Polypropylene;  $\rho_s = 875$  [kg/m<sup>3</sup>];  $U_g = 0.35$  m/s.

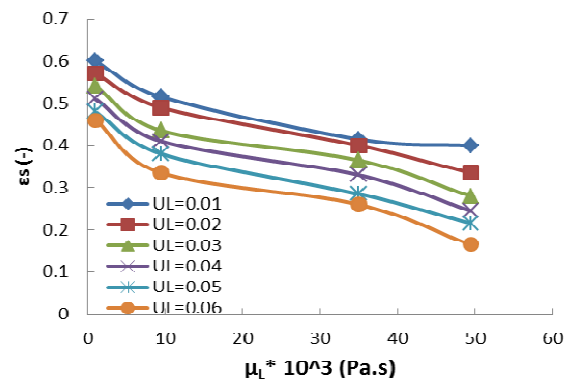


Fig. 31. Influence of  $\mu_L$  on  $\epsilon_g$  Particle: Polypropylene;  $\rho_s = 875$  [kg/m<sup>3</sup>];  $U_g = 0.35$  m/s.

### 3.4. Artificial Neural Network Model

A three layer ANN was used, a tangent sigmoid transfer function (tansig) at hidden layer and a linear transfer function (purelin) at output layer. Feed forward Levenberg- Marquardt back propagation network was used. Inside the input layer 4 neurons either in the first hidden layer there are 8 of neurons, as well as there are 4 neurons in the second hidden layer and output layer has two neurons. In the NN bed porosity model shown in figure (32 (a, b)), for training data set the  $R^2$  value is 0.990 and for testing

data set is 0.981, where the mean square error (MSE) values are  $9.4610 \times 10^{-5}$  and  $1.9099 \times 10^{-4}$  for training and testing data respectively. The ANN solid holdup model is illustrated in figure (33 (a, b)), the  $R^2$  values are 0.999 and 0.982 for training and testing data sets respectively. MSE values are  $3.8676 \times 10^{-5}$  for training data set and  $1.9099 \times 10^{-4}$  for testing data set. Figures (32 and 33) show the ANN exhibit a close prediction supported on a high value of  $R^2$  and low value of MSE. As a result, the developed NN bed porosity and solid holdup model successfully improve the prediction possibility of bed porosity and solid holdup value.

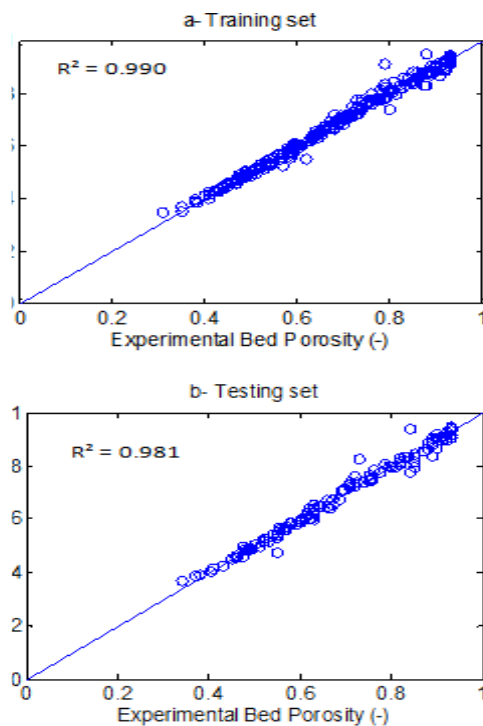


Fig. 32. The graphical output of the experimental bed porosity plotted versus neural network predicted bed porosity.

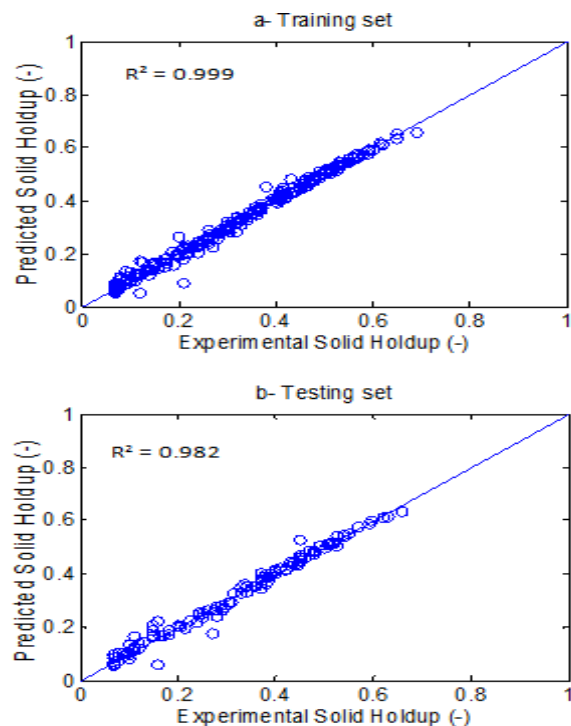


Fig. 33. The graphical output of the experimental solid holdup plotted versus neural network predicted solid holdup.

### 4. Conclusions

The bed porosity and solid holdup of viscous three-phase inverse fluidized bed were experimentally investigated for gas velocity (from 0.05 to 0.75 m/s), liquid velocity (from 0.01 to 0.06 m/s) and liquid viscosity (from  $0.97 \times 10^{-3}$  to  $49.5 \times 10^{-3}$  Pa.s) :

1. Solid holdup decreases (from 0.69 to 0.07) with increasing  $U_g$ ,  $U_L$  and  $\mu_L$ .
2.  $B_p$  increases (0.31 to 0.93) with increasing  $U_g$ ,  $U_L$  and  $\mu_L$ .
3. ANNs were used to predict the bed porosity and solid holdup.

The expected values are in an excellent

relationship with the experimental values, where the advanced model is high-fidelity and own a large capacity to predict bed porosity and solid holdup. Training data set for bed porosity model, the  $R^2$  value is 0.990 and for testing data set is 0.981, where the mean square error (MSE) values are  $9.4610 \times 10^{-5}$  for training data set and  $1.9099 \times 10^{-4}$  for testing data. For solid holdup model, the  $R^2$  values are 0.999 and 0.982 for training and testing data sets respectively. MSE values are  $3.8676 \times 10^{-5}$  for training data set and  $1.9099 \times 10^{-4}$  for testing data sets.

## 5. References

- [1] Kim, S. D. and Kang, Y., "Heat and Mass Transfer in Three-Phase Fluidized Beds; An Overview", *Chem. Eng. Sci.*, 52: 3639-3660 (1997).
- [2] Ik-Sang Shin, Sung-Mo Son, Yong Kang, Suk-Hwan Kang, and Sang-Done Kim, "Phase Holdup Characteristics of Viscous Three-Phase Inverse Fluidized Beds", *J. Ind. Eng. Chem.*, Vol. 13, No. 6, 971-978 (2007)
- [3] Jena H M, Roy G K and Mahapatra S S, "Determination of optimum gas holdup conditions in a three-phase fluidized bed by genetic algorithm", *Computers & Chemical Engineering*, 34, pp.476-484 (2009).
- [4] Muroyama, K. and L.S. Fan, "Fundamentals of Gas-Liquid-Solid Fluidization", *AIChE.J.* Vol.3, No.1, pp. 1-34 (1985).
- [5] Hee-Dong Han, Won Lee, Young-Kang Kim, Jae-Lee Kwon, Ho-Suk Choi, Yong Kang and Sang-Done Kim, "Phase Holdup and Critical Fluidization Velocity in a Three-Phase Inverse Fluidized Bed", *Korean J. Chem. Eng.*, 20(1), 163-168 (2003).
- [6] Sivalingam .A, Kannadasan .T, "Effect of Fluid Flow Rates on Hydrodynamic Characteristics of Co-Current Three Phase Fluidized Beds with Spherical Glass Bead Particles", *International Journal of Chem Tech Research*, Vol-1 (4), 851-855 (2009).
- [7] Abbas H. Sulaymon, Thamer J. Mohammed. Ali H. Jawad , "Hydrodynamic Characteristics of Three-Phase Non-Newtonian Liquid-Gas - Solid Fluidized Beds", *Emirates Journal for Engineering Research*, 15 (1), 41-49 (2010).
- [8] Aakanksha Pare, "Hydrodynamics of Three Phase Fluidized Bed Using Low Density Particles", A Thesis Submitted In Partial Fulfillment of The Requirements For The Degree of Master of Technology in Chemical Engineering, National Institute of Technology Rourkela, (2013).
- [9] Buffiere, P., and Moletta,R., "Some Hydrodynamic Characteristics of Inverse Three Phase Fluidized Bed Reactors", *Chem. Eng. Sci.*, 54, 1233-1242 (1999).
- [10] Sivasubramanian, V., Velan, M., Haribabu, K. and Deepanra , B., "Holdup Studies in IFBR for Wastewater Treatment", *Journal of Advanced Engineering Research*, Volume 1, Issue 1, pp.8-15 (2014).
- [11] Ajay, M. kumar, "Modelling The Hydrodynamic Characteristics of Gas-Liquid-Solid Fluidized Bed Using Artificial Neural Networks", A Project submitted to the National Institute of Technology, Rourkela, India, (2010).
- [12] Anant Dolas, S. L. Pandharipande and B. S. Chandak, "Modeling of Three Phase Inverse Fluidized Bed Using Artificial Neural Network", *Indian Journal of Chemical Technology*, Vol.12, pp. 327-331, May (2005).
- [13] Bimal Das, Uma Prasad Ganguly, Nirjhar Bar, and Sudip Kumar Das, "Holdup Prediction in Inverse Fluidization Using Non-Newtonian Pseudo Plastic Liquids: Empirical Correlation and ANN Modeling", *Powder Technology*, Vol. 273, pp. 83-90, March (2015).
- [14] Sozen, A., and Arcaklioglu, E., "Exergy analysis of An Ejector-Absorption Heat Transformer Using Artificial Neural Network Approach", *Journal of Applied Thermal Engineering*, Vol.27, PP.481-491 (2007).
- [15] Khalaj, G., Yoozbashizadeh, H., Khodabandeh, A., and Nazar, A., "Artificial Neural Network To Predict The Effect of Heat Treatments on Vickers Micro Hardness of Low-Carbon Nb Micro Alloyed Steels", *Journal of Neural Comput & Applic*, Vol.22, PP.879-888 (2013).
- [16] Kim, S. D. and Kang, Y., "Hydrodynamics, Heat and Mass Transfer in Inverse and Circulating Three-Phase Fluidized-Bed Reactors for Waste Water Treatment", *Stud. Surf. Sci. and Catal.*, 159: 103-108 (2006) .
- [17] Kim, S. W., Kim, H. T., Song, P. S., Kang, Y. and Kim, S. D., "Liquid Dispersion and Gas-Liquid Mass Transfer in Three-Phase Inverse Fluidized Beds", *Can. J. Chem. Eng.*, 81: 621-625 (2003).
- [18] Kang,Y., Cho,Y. J., Woo, K. J. and Kim,S. D., "Diagnosis of Bubble Distribution and Mass Transfer in Pressurized Bubble Columns With Viscous Liquid Medium", *Chem. Eng. Sci.*, 54, 4887-4893 (1999).

## التجريبية والتنبؤ باستخدام الشبكة العصبية الاصطناعية لمسامية الطبقة والمحتوى الحجمي للطور الصلب في أبراج معكوس التميع اللزج ثلاثية الطور

عامر عزيز عبدالرحمن

قسم الهندسة الكيمياءوية / الجامعة التكنولوجية  
البريد الالكتروني: [ameraa1972@yahoo.com](mailto:ameraa1972@yahoo.com)

### الخلاصة

في هذا العمل، تم حساب مسامية الطبقة والمحتوى الحجمي للطور الصلب في أبراج معكوس التميع اللزجة ثلاثية الطور باستخدام محاليل مائية للكربوكسي ميثيل السليلوز (CMC) ونوعين مختلفين من جسيمات البولي ايثيلين والبولي بروبيلين ذوات الكثافات الواطئة وبأقطار (5 ملم) في عمود من نوع (PERSPEX) ويقطر داخلي (0.092 م) مع ارتفاع (2 م). تم تحديد فعالية سرعة الغاز و السائل، لزوجة السائل، وكثافة الجسيمات على مسامية الطبقة والمحتوى الحجمي للطور الصلب. ووجد ان زيادة سرعة الغاز، سرعة السائل، ولزوجة السائل تؤدي الى زيادة مسامية الطبقة. اما المحتوى الحجمي للطور الصلب يقل عند زيادة سرعة الغاز، سرعة السائل، ولزوجة السائل. ووجد ان المحتوى الحجمي للطور الصلب للجزيئات منخفضة الكثافة تكون أعلى من الجزيئات ذي الكثافة العالية. وقد استخدم برنامج ليفينبيرك - ماركوارت العكسي للشبكة العصبية الاصطناعية لتنبؤ مسامية الطبقة والمحتوى الحجمي للطور الصلب. وظهرت القيم المتوقعة في اتفاق ممتاز مع القيم المقاسة، حيث ان النموذج المطور كان عالي الدقة ولديه نوعية كبيرة على التنبؤ.